

Rapid-acquisition pair distribution function (RA-PDF) analysis

Peter J. Chupas,^{a*} Xiangyun Qiu,^b Jonathan C. Hanson,^c Peter L. Lee,^d Clare P. Grey^a and Simon J. L. Billinge^{b*}

^aDepartment of Chemistry, State University of New York at Stony Brook, Stony Brook, New York 11794-3400, USA, ^bDepartment of Physics and Astronomy, Michigan State University, East Lansing, Michigan 48824-2230, USA, ^cDepartment of Chemistry, Brookhaven National Laboratory, Upton, New York 11793, USA, and ^dAdvanced Photon Source, Argonne National Laboratory, Argonne, Illinois 60439-4803, USA. Correspondence e-mail: pchupas@ic.sunysb.edu, billinge@pa.msu.edu

An image-plate (IP) detector coupled with high-energy synchrotron radiation was used for atomic pair distribution function (PDF) analysis, with high probed momentum transfer $Q_{\max} \leq 28.5 \text{ \AA}^{-1}$, from crystalline materials. Materials with different structural complexities were measured to test the validity of the quantitative data analysis. Experimental results are presented for crystalline Ni, crystalline α -AlF₃, and the layered Aurivillius type oxides α -Bi₄V₂O₁₁ and γ -Bi₄V_{1.7}Ti_{0.3}O_{10.85}. Overall, the diffraction patterns show good counting statistics, with measuring time from one to tens of seconds. The PDFs obtained are of high quality. Structures may be refined from these PDFs, and the structural models are consistent with the published literature. Data sets from similar samples are highly reproducible.

© 2003 International Union of Crystallography
Printed in Great Britain – all rights reserved

1. Introduction

Technologically important materials are becoming structurally more complex and disordered, and encompass a mixed range of amorphous, nanocrystalline and crystalline materials. Recently, there has been a push to characterize the structure of these materials on atomic length scales using the atomic pair distribution function (PDF) method (Egami & Billinge, 2003). This method makes use of both the diffuse and Bragg scattering components, and proves an attractive method when powder diffraction patterns prove unsatisfactory for the more traditional Rietveld analysis (Petkov, Billinge, Heizing & Kanatzidis, 2000; Petkov *et al.*, 2002). PDF analysis has been a method of choice for amorphous and liquid samples for many years (Warren, 1990). With the advent of advanced synchrotron-based X-ray sources, pulsed neutron sources and fast computing, it has more recently been successfully applied to the study of crystalline materials (Egami, 1990; Toby & Egami, 1992; Egami & Billinge, 2003).

The study of nanocrystalline and crystalline materials benefits from higher real-space resolution measurements than are typically used for amorphous or liquid samples (Petkov, Billinge, Shastri & Himmel, 2000). An important experimental requirement to obtain high real-space resolution in the PDF is to measure the structure function $S(Q)$ to a high value of scattering vector Q . Conventional high real-space resolution measurements typically make use of energy-resolving point detectors, such as high-purity germanium, that are scanned over wide angular ranges. These measurements are very slow

and generally take more than 8 h, even at a synchrotron. This, coupled with the novelty of the approach and the somewhat intensive data analysis requirements, has prevented widespread application of the technique in areas such as nanomaterials. In the present paper, we show how high-quality medium-high resolution PDFs ($Q_{\max} \leq 28.5 \text{ \AA}^{-1}$) can be obtained in a few seconds of data collection time using a two-dimensional image-plate (IP) detector. The PDFs were successfully obtained from the data using widely available data preprocessing computer packages coupled with a home-written data analysis program. These results open the way for more widespread application of the PDF technique to study the structure of nanocrystalline materials. They also open up the possibility for qualitatively new experiments to be carried out, such as time-resolved studies of local structure.

Recent developments have shown the utility of two-dimensional detector technology scattering studies of liquids. A recent report by Crichton *et al.* (2001) has made use of integrated two-dimensional IP data for *in situ* studies of scattering from liquid GeSe₂. This study, and others more recently, demonstrate the feasibility of using IPs for diffuse scattering measurements, though the measurements have been limited in real-space resolution, with $Q_{\max} \leq 13.0 \text{ \AA}^{-1}$ (Mezouar *et al.*, 2002; Kramer *et al.*, 2003), making them less suitable for the study of crystalline and nanocrystalline materials. Image plates have also been successfully used to study diffuse scattering from single crystals (Estermann & Steurer, 1998). A Debye–Scherrer camera utilizing IPs has also been tested in one of our groups and shows promise for

lower energy X-ray sources, such as laboratory and second-generation synchrotron sources (Stachs *et al.*, 2000).

Successful application of IP technology to the measurement of quantitatively reliable high real-space resolution PDFs requires that a number of issues are resolved. For example, it is necessary to correct for contamination of the signal from Compton and fluorescence intensities and for angle and energy dependencies of the IP detection efficiency (Zaleski *et al.*, 1998; Ito & Amemiya, 1991). Here, we show that high-quality medium-high real-space resolution PDFs can be obtained by applying relatively straightforward corrections. As expected, the quality of the PDFs is lower in samples comprising predominantly elements of low atomic number. Nonetheless, even the PDFs of these samples prove adequate. Studies are underway to optimize the experimental setup and our studies to date suggest that it will be possible to study low- Z materials using this approach.

A series of crystalline materials with differing structural complexities and with a wide range of scattering powers facilitates our investigation of various aspects of this technique. Here, we present results from crystalline Ni, α -AlF₃, and the layered Aurivillius-type oxides α -Bi₄V₂O₁₁ and γ -Bi₄V_{1.7}Ti_{0.3}O_{10.85}.

2. Method

All diffraction experiments were performed at the 1-ID beamline at the Advanced Photon Source (APS) located at

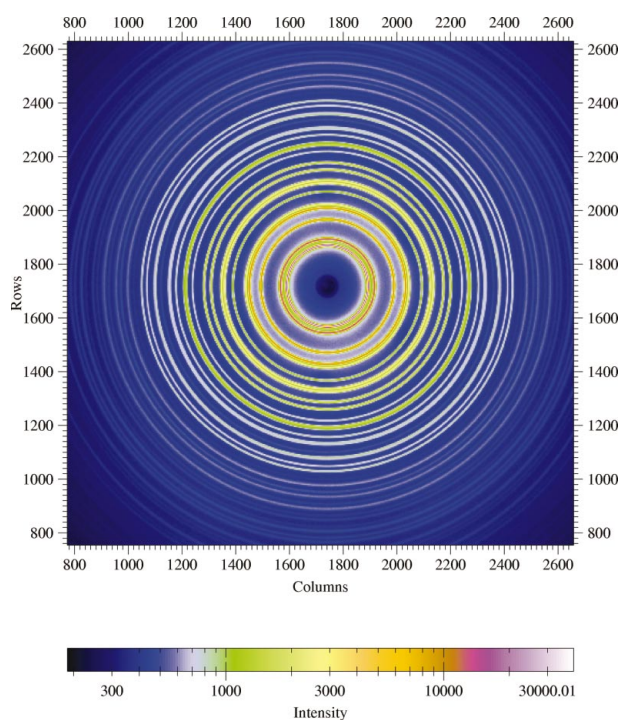


Figure 1
Two-dimensional contour plot from the Mar345 image-plate detector. The data are from nickel powder measured at room temperature with 97.572 keV incident X-rays. The concentric circles are where Debye-Scherrer cones intersect the area detector.

Argonne National Laboratory, Argonne, Illinois (USA). High-energy X-rays were delivered to the experimental hutch using a double bent Laue monochromator capable of providing a flux of 10^{12} photons s^{-1} and operating with X-rays in the energy range of 80–100 keV (Shastri *et al.*, 2002). Two energies of X-rays were used for the experiments, 80.725 keV (0.15359 Å) and 97.572 keV (0.12707 Å), with the 80.725 keV experiments being performed first. In the optics hutch, a gold foil was installed after the monochromator between two ion chambers, attenuating the flux of the beam by approximately 30.0%. Calibration of energy at 80.725 keV was achieved using the gold absorption edge as the reference.

A Mar345 image-plate camera, a round disk with a usable diameter of 345 mm, was mounted orthogonal to the beam path, with the beam centered on the IP. When operating with 80.725 keV X-rays, an LaB₆ standard was used to calibrate the sample-to-detector distance and the tilt of the IP relative to the beam path, using the software *Fit2D* (Hammersley *et al.*, 1996; Hammersley, 1998). For calibration of the IP, the wavelength was fixed to represent the gold absorption edge (0.15359 Å) at 80.725 keV. When the X-ray energy was increased from 80.725 to 97.572 keV, the sample-to-detector distance was first fixed at the value determined at the Au edge and the wavelength was calibrated using the LaB₆ standard. The IP camera was then moved closer to the sample and the new sample-to-detector distance was obtained from refinement by fixing the wavelength at 0.12707 Å. Sample-to-detector distances of 317.28 and 242.12 mm were used for collection of data, with measured Q_{\max} of 21.0 Å⁻¹ and 30.0 Å⁻¹, respectively. In practice, Q_{\max} values of 18.5 Å⁻¹ and 28.5 Å⁻¹ were used, due to corrupted data near the IP edges. The beam stop is a solid tantalum cylinder (diameter 3.1 mm), with an indentation machined to a depth of approximately 2 mm to accept the beam. With our beam-stop-to-sample distance of approximately 150 mm, the scattering angle blocked by the beam stop is less than 1°. This limits the X-ray energy-dependent Q_{\min} to approximately 0.6 Å⁻¹ with 80.725 keV X-rays. In many crystalline materials with small unit cells this is not a problem. When Bragg peaks are lost at low- Q due to this limit, a weak long-wavelength oscillation results in $G(r)$, which is not fatal but, ideally, is to be avoided.

The methods used to synthesize α -AlF₃, α -Bi₄V₂O₁₁ and γ -Bi₄V_{1.7}Ti_{0.3}O_{10.85} have been reported elsewhere (Chupas *et al.*, 2001; Kim & Grey, 2002). Ni was purchased from Alfa Aesar (99.9%, 300 mesh) and was used as received. Fine powders of all the samples were measured in flat-plate transmission geometry, with a thickness of 1.3 mm packed between Kapton foils. The beam size on the sample, as defined by the final slits before the goniometer, was 0.4 × 0.4 mm. Lead shielding before the goniometer, with a small opening for the incident beam, was used to reduce background. All raw data were integrated using the software *Fit2D* and converted to intensity versus 2θ (the angle between incident and scattered X-rays). An example of the data from Ni measured at 97.572 keV is shown in Fig. 1. The integrated data were then transferred to a home-written program, *RAPDFgetX* (unpublished), to obtain the PDF.

Distortions in intensities when using flat IPs have been addressed in single-crystal crystallography, and arise from the fact that IPs are of a finite thickness, often between 100 and 200 μm (Zaleski *et al.*, 1998; Wu *et al.*, 2002). At the high energies (≥ 60 keV) needed to measure $S(Q)$ to a high value of Q with commercial IP cameras, absorption of the X-ray photons by the phosphor is very small and most of the X-rays travel straight through the phosphor (the thin-phosphor regime). The absorption, and thus the measured intensity, is then dependent on the path length of the beam through the IP phosphor at all incident angles and can easily be corrected (Zaleski *et al.*, 1998). This oblique incidence correction assumes that the correction is equal in all directions. Thus, care was taken to ensure that the IP was mounted orthogonal to the beam. The attenuation of scattered photons after the sample, due to air absorption, is angle-dependent. This effect is negligible, due to the very small absorption of the high-energy X-rays between the sample and the detector, and is ignored. The count time is always adjusted to ensure that there are no saturated pixels in the detector. Standard corrections for multiple scattering, polarization, absorption, Compton scattering and Laue diffuse scattering were also applied to the integrated data to obtain the reduced structure function $F(Q)$ (Fig. 2*a*). Direct Fourier transformation gives the pair distribution function $G(r)$ (Fig. 2*b*). The average structure models were refined using the profile-fitting least-squares regression

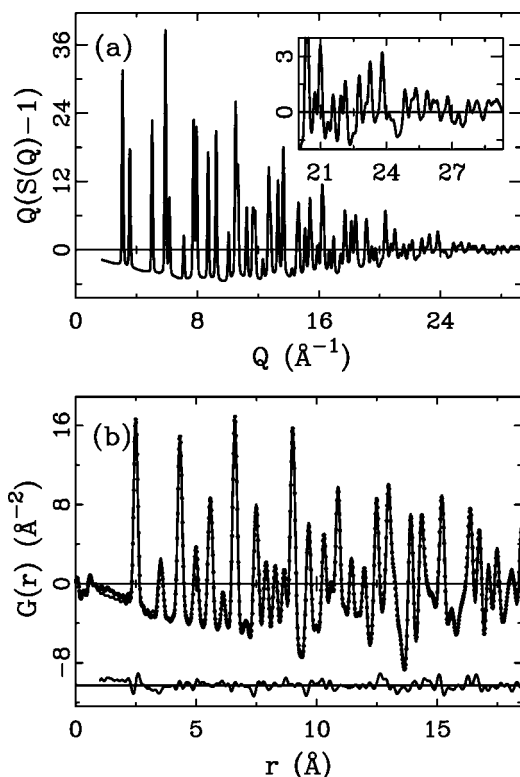


Figure 2
 (a) The experimental reduced structure function $F(Q) = Q \times [S(Q) - 1]$ of Ni powder. The inset is a magnification of the high- Q region, showing the excellent signal-to-noise ratio. (b) The experimental $G(r)$ (solid dots) and the calculated PDF from the refined structural model (solid line). The difference curve is shown offset below.

program *PDFFIT* (Proffen & Billinge, 1999). Rietveld refinements of the data were performed with *GSAS* (Larson & Von Dreele, 1987).

3. Results

All the experimental data collected from samples of Ni, α - AlF_3 , α - $\text{Bi}_4\text{V}_2\text{O}_{11}$ and γ - $\text{Bi}_4\text{V}_{1.7}\text{Ti}_{0.3}\text{O}_{10.85}$ show excellent counting statistics over the entire Q range, reflecting the significant advantage obtained by extracting one-dimensional data sets by integration of a two-dimensional area detector. Image-plate exposure time, ranging from 1 s (Ni) to 10 s (α - AlF_3), was chosen carefully for each sample to maximize the dynamic range of the IP without saturating the phosphor on the Bragg peaks. Data collection was repeated a number of times until acceptable statistical errors were observed at high- Q in the reduced structure functions, as shown in Figs. 2(*a*), 3(*a*) and 4(*a*). All the PDFs, $G(r)$, show either superior or acceptable qualities.

The first example, shown in Fig. 2, is from standard Ni powder with Q_{max} of 28.5 \AA^{-1} . The Ni PDF, $G(r)$, in Fig. 2 (*b*) appears to have minimal systematic errors, which appear as the small ripples before the first PDF peak at $r = 2.4 \text{ \AA}$. These result from imperfect data corrections and their small amplitude is a good indication of the high quality of the data. A structural model (space group $Fm\bar{3}m$) was readily refined and gave excellent agreement with the data, as shown in Fig. 2(*b*). The lattice parameter [3.5346 (2) \AA] and an isotropic thermal displacement parameter [$U = 0.005184$ (6) \AA^2] were refined. The lattice parameters reproduce the expected values given in previously published data (Billinge, 1998). In spite of the simplicity of the Ni crystal structure, the exceptional quality of both the experimental Ni PDF and the refinement indicates that the necessary data corrections of image-plate data with a high- Q range (28.5 \AA^{-1} in this case) can be carried out properly and with an acceptable level of accuracy.

The weakly scattering α - AlF_3 compound, in addition to a slightly more complex structure than Ni, presents a greater challenge to proper data correction, due to the majority contribution of Compton scattering in the high- Q region. The reduced structure function and resulting PDF are shown in Fig. 3. The data were successfully refined using a previously reported model from the literature (space group $R\bar{3}c$; Daniel *et al.*, 1990). The fit is shown in Fig. 3(*b*). The overall quality of the fit is good, with a weighted profile agreement factor (Proffen & Billinge, 1999) of 3%. The refined lattice parameters are $a = b = 4.9420$ (3) \AA and $c = 12.4365$ (2) \AA . The fractional coordinate of the F atom is $x = 0.4267$ (4). These numbers are consistent with the Rietveld refinement of the same data, which produced refined lattice parameters of $a = b = 4.9383$ (4) \AA and $c = 12.4271$ (1) \AA , and a fractional coordinate $x = 0.4287$ (4), for the F atom. Both refinements are consistent with the published data of 4.9381 (5) \AA , 12.4240 (3) \AA and 0.4309 (4), respectively (Chupas *et al.*, 2001). The successful application of PDF analysis to α - AlF_3 data indicates this technique is capable of handling weakly scattering materials and still gives reliable information.

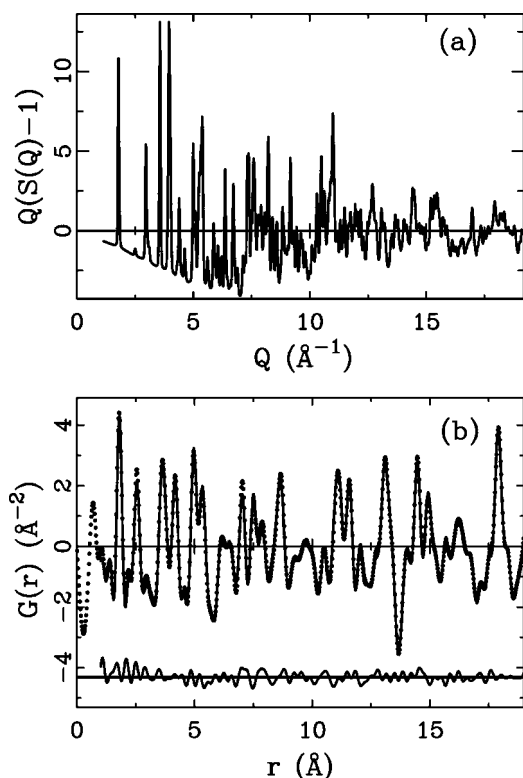


Figure 3
(a) Experimental reduced structure function $F(Q) = Q \times [S(Q) - 1]$ of α -AlF₃. (b) $G(r)$ and modeled PDF of α -AlF₃. Notations as in Fig. 2.

In addition to the highly crystalline and rather simple nickel and α -AlF₃ structures, the more complex and disordered layered Aurivillius-type oxide anion-conductors α -Bi₄V₂O₁₁ and γ -Bi₄V_{1.7}Ti_{0.3}O_{10.85} were examined. The structure is derived from the ordered Bi₄Mo₂O₁₂ structure, which contains alternating Bi₂O₂²⁺ layers spaced by corner-sharing perovskite MoO₆ layers (Kim & Grey, 2002; Yan & Greenblatt, 1995). The vanadium analogues contain significant disorder in the vanadium layers due to oxygen vacancies. Vanadium can exist in four-, five- and six-coordinate environments, inducing significant static disorder in these layers, which is further complicated by dynamic disorder resulting from the high anionic conductivity of these materials. Titanium substitution on the vanadium sites leads to the stabilization of the high-temperature γ phase. The experimentally obtained reduced structure function, $F(Q)$, of α -Bi₄V₂O₁₁ is shown in Fig. 4(a). A combined PDF and Rietveld analysis was carried out on the same data set and detailed results will be reported elsewhere. To examine the reproducibility of the systematic errors in the IP data analysis, the measured data for the compounds α -Bi₄V₂O₁₁ and γ -Bi₄V_{1.7}Ti_{0.3}O_{10.85} were compared (Fig. 4b). Clearly, the ripples in the low- r regions are rather small and highly reproducible, implying the high reliability of the PDF data, especially for comparative studies. For example, very small differences exist around the first V–O bond length of 1.80 Å, as evident in the inset of Fig. 4(b). The significant differences beyond the first peak reveal the somewhat drastic structural changes on longer length scales. This also shows that

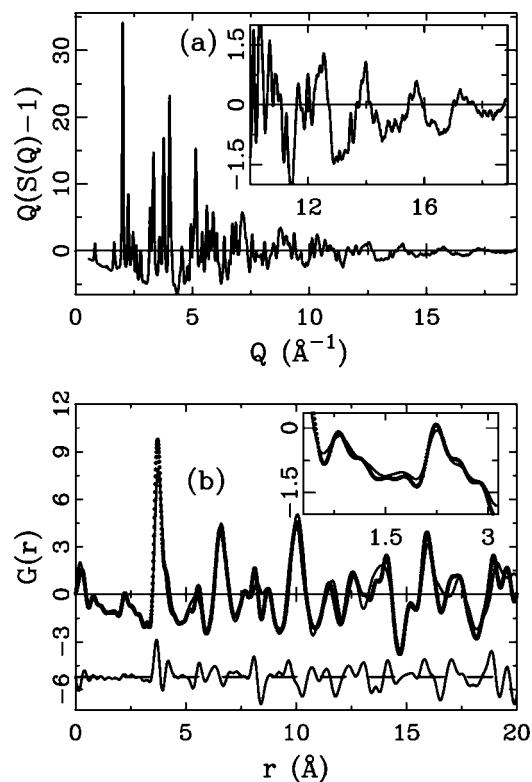


Figure 4
(a) Reduced structure function $F(Q)$ of α -Bi₄V₂O₁₁. (b) Experimentally obtained $G(r)$'s of α -Bi₄V₂O₁₁ (solid dots) and γ -Bi₄V_{1.7}Ti_{0.3}O_{10.85} (solid line). The differences between them are plotted below with an offset. Note the high reproducibility in the low- r region (also shown in the inset).

RA-PDF analysis is capable of capturing structural changes where they exist, reproducing local structures if unchanged.

4. Discussion

Previous image-plate measurements of diffuse scattering have been limited to a Q_{\max} of 13.0 Å⁻¹. In the case of the RA-PDF experiment, a much higher Q range (Q_{\max} of 30 Å⁻¹) is measured, which is necessary for PDF analysis of crystalline and nanocrystalline compounds. Here, we discuss some of the problems inherent with the use of two-dimensional detectors for PDF data collection. The good quality of the PDFs presented in this paper show that these problems are relatively minor, though they will be explicitly addressed in future experiments. The data from low- Z materials are more problematic to analyze and we have not presented any PDFs from a low- Z material measured above $Q_{\max} = 18.0$ Å⁻¹. We expect this can be resolved by addressing the problems described here.

The application of an IP camera (where readout and bleaching procedures are integrated) in these studies was chosen for two reasons. First, utilization of an IP in a flat geometry was chosen to simplify the data-correction procedure. Second, the ability to read out images in rapid succession facilitates the future implementation of time-resolved experiments. Thus, it was necessary to condense the diffraction

pattern into the usable IP area by moving to high incident X-ray energies and minimizing sample-to-IP distances. Our IP diffraction data have only moderate Q -space resolution (0.05 \AA^{-1}). This results in lost structural information in the high- r region, for example beyond $r = 40.0 \text{ \AA}$ in the Ni PDF. The majority of the loss in Q resolution comes from the finite sample size effects and could be improved by reducing the gauge volume by reducing beam size and sample thickness. Even though it may not be feasible to achieve the Q resolution of conventional PDF measurements ($\geq 0.02 \text{ \AA}^{-1}$), the current medium Q resolution does not present a serious problem in applications involving a wide range of complex structures of current interest. As we discussed, the primary effect of the moderate resolution is the loss of high- r information in the PDF. This high- r information is often neglected in analysis of PDF data.

Pushing the accessible Q range of the image plate also introduces other problematic side effects. The lack of energy resolution of the phosphor in image plates causes the inelastic component to be measured over the entire measured Q range. In conventional measurements using energy resolving detectors, the Compton and fluorescence scattering can be resolved from the elastic component. The coherent elastic scattering contains the structure information of interest but its intensity drops quickly with increasing Q . The Compton intensity can be corrected using tabulated parameters. However, the incoherent intensity increases with Q , and can be as much as five times as strong as the coherent intensity, even around $Q = 25.0 \text{ \AA}^{-1}$ (Petkov, Billinge, Shastri & Himmel, 2000). This results in signal-to-noise problems, and also a small aberration to this correction can result in a large distortion to the extracted elastic intensity. In the current correction scheme, the change in energy of the inelastically scattered Compton intensity is not explicitly included. This affects the measured intensity, due to the energy dependence of absorption and detector efficiency corrections. These are expected to be fairly small since $\Delta E/E \simeq 2.1\%$ at $2\theta = 30.0^\circ$ with an X-ray energy of 80 keV. Imperfect Compton corrections will have a more significant effect in low- Z materials where the Compton cross section is dominant. However, the current results indicate that even with the low- Z $\alpha\text{-AlF}_3$ material, the Compton scattering can be adequately corrected, at least up to $Q_{\text{max}} = 18 \text{ \AA}^{-1}$.

Data collection with image plates can be subject to quite high backgrounds, even in experiments utilizing high-energy X-rays. The detection area of an IP records all air scattering from the direct beam throughout its length, from the final scattering slits to the beam stop. As an example, in the current experiments, the measured background intensity consisted of around 80% scattering from air and 20% from the Kapton foils supporting the sample. In conventional angle-dispersive measurements, collimation after the sample position confines the visible air scattering to the small area around the sample. It is important to reduce the background scattering for quantitative PDF studies, and implementations such as extensive lead shielding around the beam path before the sample reduce, parasitic scattering. Better collimation and a helium-filled, or evacuated, flight path after the sample would also

significantly reduce the background from air scattering, but has not been implemented. Despite the non-optimized setup, the preliminary results shown here indicate quantitatively that high-quality PDFs from crystalline materials are possible using this approach, opening the way to novel experiments such as time-resolved PDF measurements. The problems addressed above will be further investigated in future measurements.

5. Conclusions

Medium-high real-space resolution PDF data analysis from crystalline materials has been performed using image-plate data and shows promising results. Comparable or even better statistics than from conventional X-ray measurements can be achieved with significantly shorter counting times. The new combination of a real-space probe and fast counting time opens up a broad field for future applications to a wide variety of materials of both scientific and technological interest. For example, PDF methods could be used to study structural changes under *in situ* conditions (Norby & Hanson, 1998), and the time development of chemical reactions and biological systems over short time scales of seconds may be studied.

This work was supported by the National Science Foundation through grant Nos. DMR-0075149, DMR-0211353 and CHE-0211029, and also by the US Department of Energy through grant Nos. DE-FG02-97ER45651, DE-FG02-96ER14681 and DE-AC02-98CH10086. John Palumbo and Namjun Kim are thanked for their help with data collection and for sample synthesis, respectively. The Advanced Photon Source is supported by the US Department of Energy through grant No. W-31-109-ENG-38.

References

- Billinge, S. J. L. (1998). In *Local Structure from Diffraction*, edited by S. J. L. Billinge & M. F. Thorpe, p. 137. New York: Plenum.
- Chupas, P. J., Ciraolo, M. F., Hanson, J. & Grey, C. (2001). *J. Am. Chem. Soc.* **123**, 1694–1702.
- Crichton, W. A., Mezouar, M., Grande, T., Stolen, S. & Grzechnik, A. (2001). *Nature*, **414**, 622–625.
- Daniel, P., Bulou, A., Rousseau, M., Noue, J., Fourquet, J. L., Leblanc, M. & Burriel, R. (1990). *J. Phys. Condens. Matter*, **2**, 5663–5677.
- Egami, T. (1990). *Mater. Trans.* **31**, 163–176.
- Egami, T. & Billinge, S. J. L. (2003). *Underneath the Bragg Peaks: Structural Analysis of Complex Materials*, edited by R. Cahn. Oxford: Pergamon Press. In the press.
- Estermann, M. A. & Steurer, W. (1998). *Phase Transitions*, **67**, 165–195.
- Hammersley, A. P. (1998). *FIT2D*. Internal Report ESRF98HA01T. European Synchrotron Radiation Facility, Grenoble, France.
- Hammersley, A. P., Svenson, S. O., Hanfland, M. & Hauserman, D. (1996). *High Pressure Res.* **14**, 235–248.
- Ito, M. & Amemiya, Y. (1991). *Nucl. Instrum. Methods A*, **310**, 369–372.
- Kim, N. & Grey, C. P. (2002). *Science*, **297**, 1317–1320.
- Kramer, M. J., Besser, M. F. N., Yang, E. R., Sordelet, D. J., Zhang, Y. & Lee, P. L. (2003). *J. Non-Cryst. Solids*, **317**, 62–70.
- Larson, A. C. & Von Dreele, R. B. (1987). *GSAS*. Report No. LAUR-86-748. Los Alamos National Laboratory, Los Alamos, NM 87545, USA.

- Mezouar, M., Faure, P., Crichton, W., Rambert, N., Sitaud, B., Bauchau, S. & Blattmann, G. (2002). *Rev. Sci. Instrum.* **73**, 3570–3574.
- Norby, P. & Hanson, J. C. (1998). *Catal. Today*, **39**, 301–309.
- Petkov, V., Billinge, S. J. L., Heizing, J. & Kanatzidis, M. G. (2000). *J. Am. Chem. Soc.* **122**, 11571–11576.
- Petkov, V., Billinge, S. J. L., Larson, P., Mahanti, S. D., Vogt, T., Rangan, K. K. & Kanatzidis, M. G. (2002). *Phys. Rev. B*, **65**, 092105.
- Petkov, V., Billinge, S. J. L., Shastri, S. D. & Himmel, B. (2000). *Phys. Rev. Lett.* **85**, 3436–3439.
- Proffen, T. & Billinge, S. J. L. (1999). *J. Appl. Cryst.* **32**, 572–575.
- Shastri, S. D., Fezzaa, K., Mashayekhi, A., Lee, W.-K., Fernandez, P. B. & Lee, P. L. (2002). *J. Synchrotron Rad.* **9**, 317–322.
- Stachs, O., Gerber, T. & Petkov, V. (2000). *Rev. Sci. Instrum.* **71**, 4007–4009.
- Toby, B. H. & Egami, T. (1992). *Acta Cryst. A* **48**, 336–346.
- Warren, B. E. (1990). *X-ray Diffraction*. New York: Dover.
- Wu, G., Rodrigues, B. L. & Coppens, P. (2002). *J. Appl. Cryst.* **35**, 356–359.
- Yan, J. & Greenblatt, M. (1995). *Solid State Ionics*, **81**, 225–233.
- Zaleski, J., Wu, G. & Coppens, P. (1998). *J. Appl. Cryst.* **31**, 302–304.